IJCCSM
18,1

Received 27 July 2025
Revised 12 December 2025
24 March 2026
Accepted 25 March 2026

Climate change dominance shifting China's semi-arid/semi-humid boundary since 1961

Yang Li
Faculty of Geographical Science and Engineering, College of Geographical Sciences, Henan University, Zhengzhou, China, and Key Laboratory of Geospatial Technology for the Middle and Lower Yellow River Regions, Ministry of Education, Henan University, Kaifeng, China

Jiayao Wang and Yuanxiang Li
Faculty of Geographical Science and Engineering, College of Geographical Sciences, Henan University, Zhengzhou, China, and

Yaochen Qin
Faculty of Geographical Science and Engineering, College of Geographical Sciences, Henan University, Zhengzhou, China; Key Laboratory of Geospatial Technology for the Middle and Lower Yellow River Regions, Ministry of Education, Henan University, Kaifeng, China and Key Research Institute of Yellow River Civilization and Sustainable Development and Collaborative Innovation Center on Yellow River Civilization jointly built by Henan Province and Ministry of Education, Henan University, Kaifeng, China

Abstract

Purpose – The 400 mm isohyet, as the boundary between semi-humid and semi-arid regions, has severe spatiotemporal variations that inevitably generate a series of economic, social and ecological impacts. However, traditional studies primarily measured the coarse variations (latitude and longitude) of the 400 mm isohyet. Due to the complexity and variability of annual isohyet fluctuations, finescale changes (multidirection and magnitude) remain difficult to quantify. Thus, this study aims to systematically quantify the fluctuation characteristics of the 400 mm isohyet.

Design/methodology/approach – To address this limitation, a high-precision long-term precipitation product was constructed and evaluated. In addition, this study introduced a boundary fluctuation detection method to quantitatively analyze the spatiotemporal dynamics of the isohyet.

Findings – The 400 mm isohyet in the eastern region of China exhibited a significant westward shift (−0.036° yr^{-1}, $p < 0.05$) and a slight southward shift (−0.025° yr^{-1}). The most pronounced oscillations of the decadal 400 mm isohyet occurred in the border areas of Heilongjiang, Jilin and Inner Mongolia. Temporally, between the 1980s and the 2000s, the isohyet in Northeast China clearly retreated southeastward, reflecting a transition toward a warmer and drier climate. In contrast, during the 2010s, the isohyet in Northeast China region, the

Funding: This work was supported by the National Natural Science Foundation of China [grant numbers: 42301104 and 42171295].

International Journal of Climate Change Strategies and Management
Vol. 18 No. 1, 2026
pp. 280-295
Emerald Publishing Limited
1756-8692
DOI 10.1108/IJCCSM-07-2025-0237

Inner Mongolia and the Great Wall region, the Loess Plateau region and the Qinghai-Tibet Plateau advanced northwestward compared to the 2000s, indicating a shift toward a warmer and wetter climate.

Practical implications – This study strengthens and enhances the understanding of the spatiotemporal variation characteristics and patterns of agro-pastoral boundaries in the context of climate change, providing a scientific basis for climate change modeling, mitigation and adaptation strategies.

Originality/value – This study introduced a refined method to detect the spatiotemporal characteristics of 400 mm isohyet variations, overcoming previous challenges in capturing multidirectional changes in isohyet and filling a gap in the quantitative detection of geographical boundaries with temporal and spatial fluctuation characteristics.

Keywords 400 mm isohyet, Rasterization, Temporal and spatial variation, Multi-azimuth, China

Paper type Research paper

1. Introduction

The Sixth Assessment Report of the Intergovernmental Panel on Climate Change (IPCC) explicitly states that climate change is intensifying the global water cycle and altering precipitation patterns, resulting in more frequent extreme rainfall events and increasingly severe droughts (Treppiedi *et al.*, 2025; IPCC, 2021). Accordingly, the study of dynamic changes in natural geographic systems has become a frontier topic in geographical research (Zheng *et al.*, 2016). Especially, the accurate description of the spatial and temporal distribution of precipitation is of great importance in the field of climatology (Chen *et al.*, 2024). The 400 mm isohyet (separating semi-arid and semi-humid regions) serves as a critical climatic boundary and essential indicator of climate change and natural regionalization (Che *et al.*, 2020; Yuan *et al.*, 2014). In particular, the 400 mm isohyet is a crucial boundary between semi-arid and semi-humid regions, whose spatial position fluctuates significantly over time (Zhao *et al.*, 1993). These fluctuations inevitably affect the distribution of regional water resources, triggering a series of resource-related ecological and socioeconomic impacts (Wang *et al.*, 2005). In China, the area east of the 400 mm isohyet encompasses approximately 90% of the country's cropland and population, as well as 96% of its gross domestic product, covering 43% of the country's total land area (Gao *et al.*, 2020). In contrast, the area west of this isohyet exhibits significant variability in terms of aridity and humidity (Wang *et al.*, 2008), posing severe threats to the ecological security and sustainable development of northwestern China. Therefore, it is crucial to understand the spatiotemporal variability of the 400 mm isohyet in China to identify climate-induced shifts in dry and wet conditions in environmentally sensitive regions, as well as to guide ecological protection and improvement efforts. Furthermore, the Chinese regions that are spatially affected by the 400 mm isohyet are key areas sensitive to climate change and vulnerable to ecological disturbances. These regions are critical zones where terrestrial ecosystems respond to both climate change and human activities (Liu *et al.*, 2007). The spatiotemporal distribution of natural elements within these areas is highly uneven, making them some of the most unstable regions in the human–environment system. Under the combined effects of climate change and human activities, environmental evolution within these areas often exhibits varying degrees of irreversibility. Accordingly, the accurate identification of the key regions characterized by long-term fluctuations in the 400 mm isohyet is a fundamental prerequisite for the restoration and protection of ecologically fragile areas in China.

Historical observations and climate model simulations indicate that in China, the extent of global arid and semi-arid regions has been continuously expanding over the past 60 years. This trend is expected to accelerate under scenarios of ongoing global warming (Huang *et al.*, 2016a; Huang *et al.*, 2017). Simultaneously, global warming has intensified the rate of the water cycle (Liepert and Romanou, 2005), exerting significant impacts on both global and regional precipitation patterns (Hsu and Fueglistaler, 2025). This acceleration is projected to exacerbate water scarcity in arid and semi-arid regions (Held and Soden, 2006), thereby driving spatiotemporal fluctuations in the 400 mm isohyet.

Currently, the study of the spatial variation characteristics of isohyets remains limited due to constraints in the quantity, accuracy and methodologies of observational data (Andrew and Bill, 2002). Some researchers used surface observations (Yuan *et al.*, 2014), gridded precipitation data sets (Che *et al.*, 2020), and global reanalysis data (Gao *et al.*, 2020) to conduct exploratory analyses of the longitudinal and latitudinal variations of the 400 mm isohyet in China at national and regional scales. These studies revealed a significant periodicity and spatial heterogeneity in the spatial fluctuations of the 400 mm isohyet. More in detail, Gao *et al.* (2020) identified pronounced fluctuations in the eastern and western segments of the 400 mm isohyet, whereas the central segment remained relatively stable. In different climate change scenarios in the future, the weighted mean longitude of the eastern and western segments of the 400 mm isohyet is projected to decrease significantly, while the central segment is expected to remain relatively stable. At the regional scale, the 400 mm isohyet in the Yellow River Basin exhibited a significant trend of eastward and southward migration from 1956 to 2000, with the former direction being more prominent (Wang *et al.*, 2005). In northern China, from 1960 to 2016, the mid-eastern segment of the isohyet displayed a westward and southward migration.

Overall, previous studies used the weighted mean coordinate changes of the 400 mm isohyet, derived from ground-based precipitation observation data, to characterize its shift. These studies revealed pronounced sectional fluctuation characteristics of the isohyet, although with varying degrees of inconsistency in determining its migration direction and distance. These discrepancies may be due to the fact that the weighted average method quantifies changes only along the longitudinal and latitudinal directions, making it challenging to precisely measure shifts in other directions. In fact, the spatial migration of the isohyet exhibits notable sporadic and multidirectional characteristics. Currently, the majority of existing studies focused on the detection of changes in the 400 mm isohyet along longitudinal and latitudinal directions, lacking a comprehensive depiction of its shifts in other orientations. In addition, the direction and magnitude of isohyet displacement derived by different researchers often showed discrepancies. Therefore, there is an urgent need to develop detection methods capable to accurately measure changes in isohyet across multiple orientations.

To address this need, this study used a boundary fluctuation detection method to quantify the spatial shifts of the isohyets. It comprehensively investigated the characteristics of the 400 mm isohyet in China since the 1960s, addressing previous challenges in depicting multidirectional changes and filling the methodological gap in quantifying spatiotemporal changes of linear geographic elements. The three primary research objectives of this study were as follows:

(1) to generate a high-resolution, long-term precipitation gridded data set at the kilometer scale, driven by high-density, long-sequence meteorological station observations and using a thin-plate spline interpolation model with elevation as a covariate;

(2) to propose a coupled wavelet analysis and boundary fluctuation detection method for the precise detection of the spatiotemporal fluctuation characteristics of the 400 mm annual isohyet in China since 1961; and

(3) to compare the spatial differences in direction and magnitude of interannual and decadal variations in the isohyet, and to accurately identify regions with high-amplitude isohyet fluctuations.

The main contribution of this study lies in the construction of a refined approach to detect isohyet fluctuations, which provides methodological support for the quantitative and detailed assessment of the spatiotemporal fluctuation characteristics of geographic boundaries.

2. Research data and methods

2.1 Overview of the study area

This study selected various agricultural zones in China for statistical and analytical purposes (Figure 1). In relation to regional divisions, the southeastern regions of China are characterized by semi-humid and humid climates, while the northwestern regions are dominated by arid and semi-arid climates (Du *et al.*, 2023; Zheng *et al.*, 2013). The geographical distribution and the variability of rainfall in China are highly complex and diverse. Generally, rainfall in southeastern China is significantly higher than in the northwest.

2.2 Research data

2.2.1 Meteorological stations data set. This study used daily precipitation data from more than 2,400 meteorological observation stations since 1961, compiled by the National Meteorological Information Center of the China Meteorological Administration (CMA) (https://data.cma.cn/), to conduct a refined investigation of isohyetal fluctuations. Moreover,

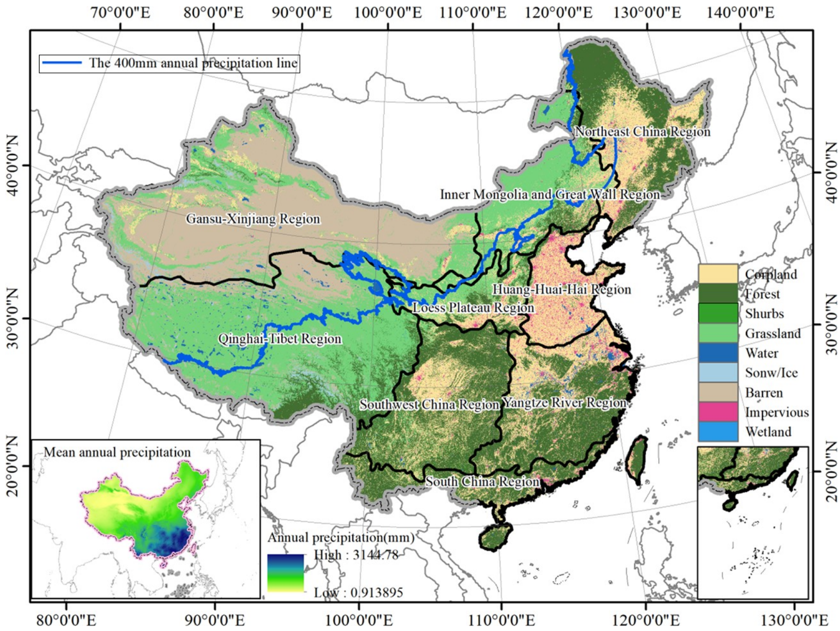

Figure 1. Map of the study area

Note: NECR = Northeast China region; MGR = Inner Mongolia and Great Wall region; LPR = Loess Plateau region; HHHR = Huang-Huai-Hai region; QTR = Qinghai-Tibet region; GXR = Gansu-Xinjiang region; SWCR = Southwest China region; YRR = Yangtze River region; SCR = South China region

Source: Authors' own work

to ensure effective interpolation and maintain stable interpolation accuracy, station data were subjected to screening and quality control procedures, and data imputation was performed for the missing periods.

2.2.2 Global precipitation grid data set. This study used observational data from over 2,000 meteorological stations across China, incorporating terrain factors to spatialize precipitation data. On the one hand, the spatialized multiyear precipitation data set for China was evaluated using observational data from reserved meteorological stations. On the other hand, the accuracy of the spatialized precipitation data produced in this study was compared with that of leading global precipitation gridded products to verify the reliability of the data set. Key information on the eight mainstream precipitation products included in the comparison is summarized in Table S1 in Supplementary Material.

2.3 Research methods

2.3.1 Meteorological data interpolation method. The thin-plate smoothing spline function has been proven to be suitable for the gridding of long-term climate data series (Zhao *et al.*, 2019). This method provides a set of statistical parameters to determine error sources and evaluate interpolation quality. It also supports the simultaneous interpolation of multiple surfaces, offering a high computational efficiency and ease of operation (Hutchinson and Xu, 2013). The theoretical model of thin-plate smoothing spline interpolation was expressed as follows (Wahba and Wendelberger, 1980):

$$z_i = f(x_i) + b^T y_i + e_i (i = 1, 2 \cdots, N) \tag{1}$$

where z_i is the dependent variable at the *i*th point in the interpolation space; x_i is the d-dimensional vector of the independent variables; y_i is the p-dimensional vector of the independent covariates; *f* is the unknown smooth function of x_i; *b* is a p-dimensional vector regarding the y_i coefficient; e_i is the random error term, with an expected value of 0 and a variance of $w_i\sigma^2$; w_i is the known local loudness coefficient of variation of the weight; and σ^2 is the error variance.

When $p = 0$, the model can be simplified into an ordinary thin disk smooth spline function, and the function *f* and the coefficient vector *b* can be determined using the least squares estimation, as follows:

$$\sum_{i=1}^{N} \left(\frac{z_i - f(x_i) - b^T y_i}{w_i} \right)^2 + \rho Jm(f) \tag{2}$$

where $J_m (f)$ is the roughness measure function for the function $f(x_i)$, defined as the integral of the *m*th order partial derivatives of the function *f*; and ρ is the smoothing parameter. When ρ approaches 0, the fitted function approaches exact interpolation; when ρ approaches infinity, the fitted function converges to a least squares polynomial, with the degree of the polynomial determined by the order m of the roughness measure function.

2.3.2 Criteria to evaluate the best interpolation model. Based on Lu and Lu (2019), the following benchmarks were used to select the optimal spatial interpolation model for precipitation data: the minimum of square root of generalized cross-validation (RTGCV); the minimum of Signal-to-Noise Ratio; a signal value present in less than half the number of stations; and the absence of the symbol "*" in the model validation report.

2.3.3 Evaluation methods of interpolation accuracy. This study evaluated the interpolation accuracy of China grid precipitation (CPG) data based on ground observation data, using the commonly used metrics for climate data interpolation model evaluation, such as the correlation coefficient (R), the Mean Absolute Error (MAE), the Mean Relative Error (MRE) and the Root Mean Square Error (RMSE) (Liu *et al.*, 2012). The calculation formulas are as follows:

$$R = \frac{\sum_{i=1}^{n}(x_i - \bar{x})(y_i - \bar{y})}{\sqrt{\sum_{i=1}^{n}(x_i - \bar{x})^2}\sqrt{\sum_{i=1}^{n}(y_i - \bar{y})^2}} \tag{3}$$

$$RMSE = \frac{\sqrt{\sum_{i=1}^{n}(x_i - y_i)^2}}{\mathrm{n}} \tag{4}$$

$$MRE = \frac{\sum_{i=1}^{n}|(x_i - y_i)|*100\%}{\sum_{i=1}^{n}|(x_i)|} \tag{5}$$

$$\mathrm{MAE} = \frac{\sum_{i=1}^{n}|x_i - y_i|}{n} \tag{6}$$

where x_{i} and y_{i} represent the simulated precipitation data and station data, respectively; $\bar{x}$ is the mean of the simulated precipitation data; $\bar{y}$ is the mean of the station−observed data; and n is the number of stations.

2.3.4 Methods to measure variations of the 400 mm isohyet. This study used CPG data to detect isohyet variations. To this purpose, the interannual and decadal variations of the isohyet were detected using the weighted average coordinates method and the fine-grained multidirectional variation detection method:

2.3.4.1 Weighted average coordinates method.

- Based on the spatialized gridded precipitation data, this study extracted the 400 mm isohyet for China for each year, removing short arc segments scattered across the region and selecting spatially continuous isohyet arcs as the 400 mm isohyet for the corresponding year. Subsequently, the 400 mm isohyet was discretized, and the weighted average longitude and latitude coordinates of the discrete points were calculated (Yuan *et al.*, 2014). The spatial migration characteristics of the annual isohyet were represented by the changes in the weighted average coordinates.

2.3.4.2 Fine-grained detection of multidirectional variations in the isohyet.

- Thanks to its advantages, including good simulation effect, flexible parameter setting, and accurate statistics, the Digital Shoreline Analysis System (DSAS) is widely used in the quantitative study of the spatiotemporal dynamic change characteristics of linear geographic elements (Amrouni *et al.*, 2019). Therefore, this study applied the DSAS to assess the variation of 400 mm precipitation isohyet in China. First, as the southeastern boundary was used as the baseline in this study, the distances of the isohyets in different periods were buffered, and the southeastern or northwestern boundary of their minimal enclosing polygon were identified as the reference baseline for the detection of distance changes. Second, equidistant perpendicular segments were drawn along the baseline, ensuring they intersect the isohyets of different periods. Third, the distances from the intersection points of the isohyets of each period to the baseline along the equidistant perpendiculars were calculated. Finally, the variation distances and directional parameters of isohyets between every two periods were computed along each equidistant perpendicular, enabling a precise measurement of the multidirectional variation magnitudes of the 400 mm isohyet in China.

3. Results

3.1 Assessment of the accuracy of precipitation products

3.1.1 Diagnostic information on the validity of interpolation models. Figure 2 presents the diagnostic information of the interpolation model for annual precipitation in China since 1961. The Signal values ranged from 545.30 to 992.20, with a multiyear mean of 821.4, which was less than half the number of observation stations, thereby confirming the effectiveness of the surface model used in precipitation gridding. The RTGCV values varied between 1.68 and 2.12, with an average of 1.86. Hutchinson and Xu (2013) suggested that the asymmetry in the spatial distribution of precipitation data makes the MRE more suitable for accuracy evaluation. A common criterion for reliable interpolation results is that MRE < 10%. In this study, the MRE values of the precipitation interpolation model ranged from 5.73% to 7.11%, with an average of 6.30%, indicating that the gridded precipitation data obtained through interpolation in this study exhibited high accuracy and reliability. Moreover, as shown in Table S2 in Supplementary Material, the correlation coefficient R values ranged between 0.95 and 0.98, with a multiyear average of 0.97. The multiyear averages for MRE, MAE and RMSE were 9.20%, 79.72 and 114.67, respectively.

3.1.2 Correlation between surface-observed precipitation and gridded data sets. As illustrated in Figure 3, a high degree of consistency was observed between the nine gridded precipitation data sets and surface observations ($p < 0.01$). More in detail, the CPG data, which in this study were obtained through interpolation, showed the highest correlation with surface observations, with an R-value of 0.96 ($p < 0.01$). Overall, the CPG data set, derived from the spatialization of precipitation data from over 2,000 meteorological stations in China, achieved the highest accuracy.

3.1.3 Taylor diagram of surface-observed precipitation and gridded data sets. Figure 4(a) presents the time series variation curves for station data and the eight gridded precipitation products. The annual precipitation in China exhibited significant fluctuations. More in detail, CPG exhibited the closest time series trend to surface-

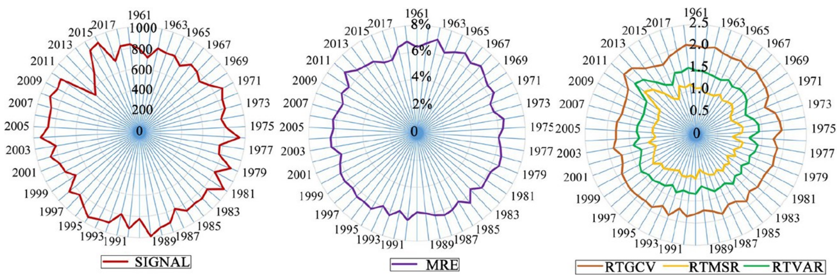

Figure 2. Generalized cross-validation of the spatial interpolation model for annual precipitation in China

Source: Authors' own work

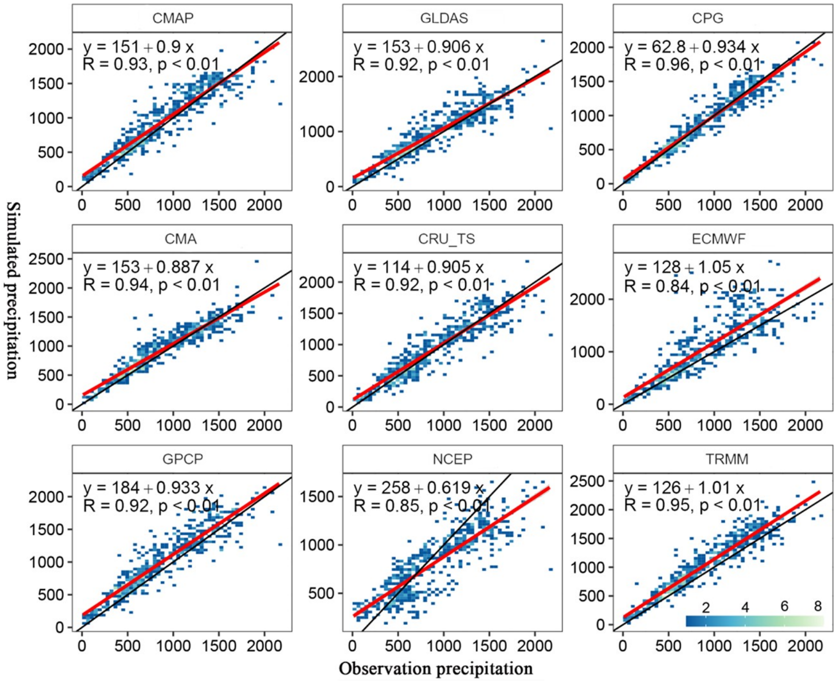

Figure 3. Density scatter plot of station observation precipitation data and interpolation data
Source: Authors' own work

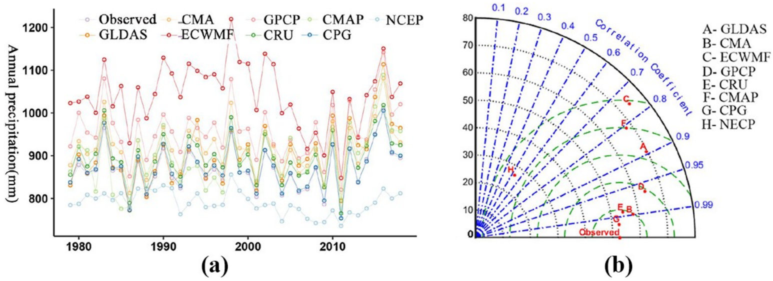

Figure 4. Taylor diagram of station observation data and mainstream precipitation products
Source: Authors' own work

observed data, while European Centre for Medium-Range Weather Forecasts and National Centers for Environmental Prediction showed the worst consistency. As shown in Figure 4(b), the CPG had the highest correlation with observed data ($R > 0.99$), followed by CMA and Climatic Research Unit; this indicates that the gridded precipitation data set developed in this study had superior accuracy compared to existing mainstream precipitation products.

3.2 Shift of the semi-arid/semi-humid boundary in China

3.2.1 National scale. Figure 5(a) and (b), presents the interannual variations of the weighted average longitude and latitude of the 400 mm isohyet. Both the longitude and latitude of the isohyet exhibited a decreasing trend, with rates of change of −0.03° yr^{-1} and −0.008° yr^{-1}, respectively. This indicates that the 400 mm isohyet in China has been generally shifting westward, with a secondary southward migration, thus reflecting a spatial migration pattern dominated by westward movement and supplemented by southward movement.

3.2.2 East-west regional scale. The weighted average longitude coordinate of the 400 mm isohyet in China was used as a boundary to divide the country into two regions: the western region (from longitude 81.49° E to 104.35°E) and the eastern region (from longitude 104.35°E to 129.57°E). The spatial migration characteristics of the isohyet were measured from a regional perspective [Figure 5(c)–(g)]. Due to the influence of factors such as topography, land-ocean location and monsoon, a significant difference was observed in the spatial migration of the 400 mm isohyet between the two regions. In the eastern region, the weighted average longitude of the isohyet significantly decreased (−0.036° yr^{-1}, $p < 0.05$), while the latitude showed no significant decreasing trend (−0.025° yr^{-1}). In contrast, the western region exhibited an increasing trend in both longitude (0.004° yr^{-1}) and latitude

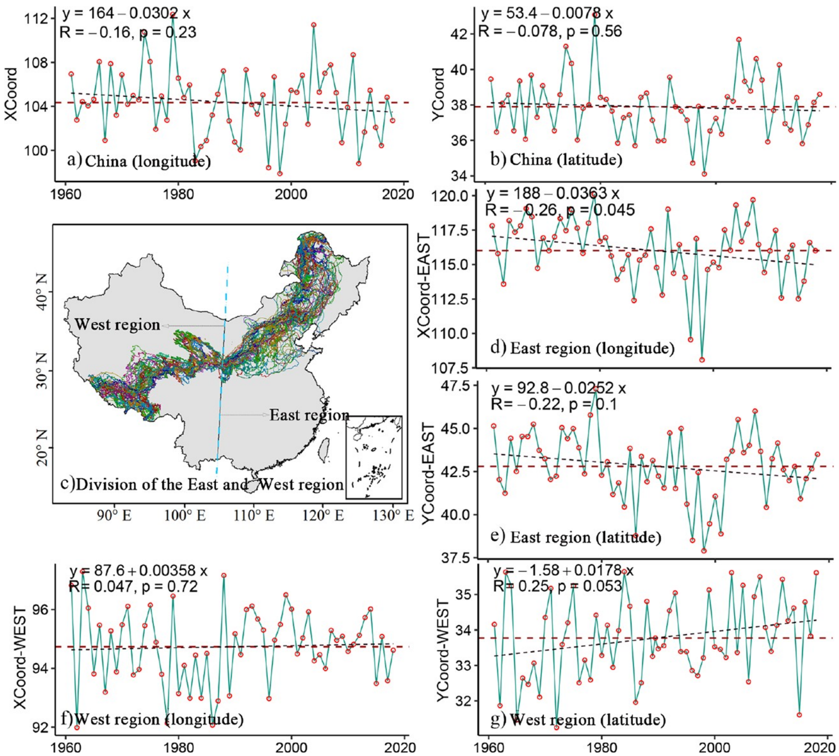

Figure 5. Interannual variation of the weighted average longitude and latitude of the 400 mm precipitation contour in China

Source: Authors' own work

(0.018° yr^{-1}, $p < 0.1$). Furthermore, the fluctuation in the eastern region was considerably stronger than in the western region. Similarly, the weighted average coordinates of the 400 mm isohyet and their longitudinal and latitudinal trends were calculated for different agricultural regions (Table S3 in Supplementary Material).

3.3 Decadal 400 mm isohyet changes across agricultural regions

3.3.1 Changes of the decadal 400 mm isohyet in China. As shown in Figure S1, the decadal 400 mm isohyet in China exhibited a generally stable pattern with localized fluctuations, showing distinct segmented oscillation characteristics. The most intense oscillations occurred at the intersection of Heilongjiang, Jilin and Inner Mongolia, followed by the Qinghai-Tibet Plateau. Figure 6 illustrates the decadal directional changes of the 400 mm isohyet across agricultural regions in China. Since the 1960s, the 400 mm isohyet followed an overall oscillation pattern of advancement and retreat along the southeast-northwest axis. The Middle and Lower Inner Mongolia and Great Wall region (MGR) exhibited the most pronounced fluctuations, followed by the Northeast China region (NECR) and Qinghai-Tibet region (QTR), while the Loess Plateau region (LPR) remained relatively stable. During the 1970s–1980s, the isohyet in the QTR shifted significantly toward the southwest and southeast. In the 1980s–1990s, it displayed a combined southwestward and northwestward movement. From the 1990s to 2000s, the isohyet in the NECR migrated noticeably toward the northeast, while in the 2000s–2010s, it shifted prominently toward the southwest.

Specifically, during the 1960s–1970s, the 400 mm isohyet in the NECR and MGR exhibited an alternating pattern of northwestward advancement and southeastward retreat. In contrast, the LPR and QTR experienced relatively stable conditions with localized fluctuations. From the 1970s to the 1980s, the isohyet generally showed a southeastward retreat in the MGR, QTR and LPR. However, certain areas within the MGR witnessed a significant advancement into the northwest interior, indicating extreme spatial precipitation imbalance and sharp transitions between droughts and floods. During the 1980s–1990s, the isohyet predominantly advanced northwestward in the MGR and NECR, while a retreat was observed in the QTR. From the 1990s to the 2000s, the isohyet exhibited a general retreat in the NECR, MGR and LPR, while the QTR experienced a pronounced northwestward advancement. In addition, the NECR shifted notably toward the southwest. In the 2000s–2010s, the isohyet advanced northwestward across the NECR, MGR, LPR and QTR.

3.3.2 Shifting distances of the 400 mm isohyet on a decadal scale. Similarly, Table 1 reveals a clear spatiotemporal variability in the shifting distances of the 400 mm isohyet on a decadal scale. More in detail, the largest northwestward advancement occurred in the NECR during the 2000s-2010s, with an average distance of 159.72 km. Conversely, the greatest southeastward retreat was observed in the NECR during the 1990s–2000s, with a magnitude of −193.04 km.

Distance of advancement toward the northwest. In the 1960s–1970s, the NECR exhibited the greatest advancement, with an average distance of 41.95 km, followed by the MGR (20.09 km) and the QTR (19.37 km), while the LPR showed a minimal advancement. During the 1970s–1980s, the NECR again had the highest advancement, averaging 97.76 km, followed by the QTR (31.38 km) and the MGR (28.87 km), with the LPR recording the smallest advancement (2.10 km). During the 1980s–1990s, the MGR led with an average advancement of 105.61 km, followed by the QTR (86.91 km), while the LPR recorded the smallest value (15.85 km). During the 1990s–2000s, the QTR showed the greatest advancement, with an average of 41.53 km and a maximum of 130.43 km, followed by the MGR (16.69 km) and the LPR (9.43 km). The NECR, however, retreated southeastward.

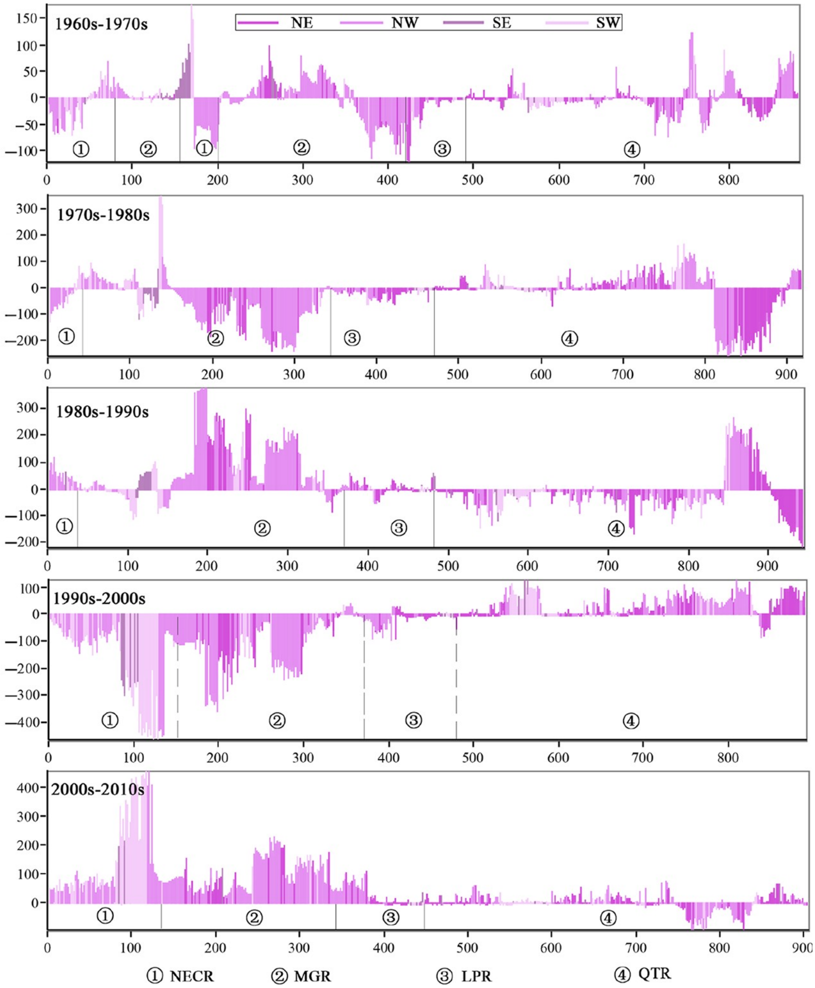

Figure 6. Interdecadal drift of the 400 mm precipitation isohyet in China

Source: Authors' own work

Finally, during 2000s–2010s, the NECR experienced the most significant advancement, with an average of 159.72 km and a maximum of 460.15 km, followed by the MGR (93.90 km) and the LPR (26.63 km), while the QTR recorded the smallest advancement (13.81 km).

Distance of retreat toward the southeast. During the 1960s–1970s, the QTR had the largest retreat, averaging −91.97 km, followed by the MGR (−87.85 km) and the NECR (−44.88 km), while the LPR showed the smallest retreat (−15.57 km). During the 1980s–1990s, the NECR had the greatest retreat, averaging −54.50 km, followed by the QTR (−37.77 km), while the LPR recorded the smallest retreat (−15.32 km). During the 1990s-2000s, the NECR had the most significant retreat, averaging −193.04 km, followed by the MGR (−103.85 km), while the LPR had the smallest retreat (−21.52 km). Finally, during the

Table 1. Changes in the distance of advancement and retreat of the 400 mm isohyet on a decadal scale

		Distance of advancement toward the northwest (unit: km)				Distance of retreat toward the southeast (unit: km)			
Time	Region	Average	Max.	Min.	Median	Average	Max.	Min.	Median
1960s–1970s	NECR	41.95	177.66	0.38	28.04	−43.41	−0.08	−90.64	−48.36
	LPR	0.16	0.49	0.01	0.15	−19.01	−0.03	−121.70	−3.88
	MGR	20.09	101.05	0.00	15.25	−36.76	0.00	−110.67	−40.87
	QTR	19.37	126.07	0.00	8.23	−13.62	−0.02	−71.18	−8.57
1970s–1980s	NECR	97.76	354.35	1.30	51.62	−44.88	−0.75	−124.67	−48.82
	LPR	2.10	5.99	0.14	0.17	−15.57	−0.04	−57.70	−9.72
	MGR	28.87	101.01	0.69	27.11	−87.85	0.00	−235.44	−71.68
	QTR	31.38	171.93	0.04	19.71	−91.97	−0.02	−260.68	−48.31
1980s–1990s	NECR	59.67	125.23	13.01	55.05	−54.50	−29.67	−81.01	−55.82
	LPR	15.85	64.48	0.03	11.13	−15.32	−0.05	−43.68	−12.84
	MGR	105.61	382.62	0.00	59.40	−23.27	0.00	−107.06	−12.13
	QTR	86.91	270.63	0.02	54.38	−37.77	−0.01	−220.68	−23.10
1990s–2000s	NECR	0.00	0.00	0.00	0.00	−193.04	−3.72	−464.43	−112.94
	LPR	9.43	36.43	0.16	2.26	−21.52	−0.02	−87.89	−9.65
	MGR	16.69	42.63	0.16	12.08	−103.85	0.00	−354.01	−92.26
	QTR	41.53	130.43	0.00	36.42	−30.72	−0.01	−76.19	−37.00
2000s–2010s	NECR	159.72	460.15	0.21	87.98	0.00	0.00	0.00	0.00
	LPR	26.63	111.81	0.11	7.10	−0.07	−0.01	−0.12	−0.07
	MGR	93.90	337.49	2.69	78.61	0.00	0.00	0.00	0.00
	QTR	13.81	78.32	0.07	6.49	−31.72	−0.02	−96.47	−23.38

2000s–2010s, the QTR recorded the greatest retreat (−31.72 km), followed by the LPR (−0.07 km), while the MGR and the NECR experienced a minimal retreat.

4. Discussion

During the study period, the 400 mm precipitation isohyet in China shifted westward and southward at a rate of $-0.03\,yr^{-1}$ and $-0.008\,yr^{-1}$ in the longitudinal and latitudinal directions, respectively. The interdecadal 400 mm precipitation isohyet in China also advanced northwestward in the QTR. This finding is in line with Gao *et al.* (2020), who similarly concluded that, based on CNgrid and Global Precipitation Climatology Centre precipitation data from 1961 to 2019, the 400 mm precipitation isohyet in the Tibetan Plateau region (west of 93°E) showed a significant westward shift. This observation corroborates the results of other studies indicating a trend of warming and increasing humidity in the region (Ding *et al.*, 2023; Li *et al.*, 2025). During the majority of the periods investigated, the interdecadal 400 mm precipitation isohyet retreated significantly southeastward in the MGR and the LPR, with the MGR showing larger fluctuations compared to other regions. Similar trends of expansion in the drought area have also been noted in other regions (Huang *et al.*, 2016a; Prăvălie *et al.*, 2019). The trend of drying up of the climate in the Loess Plateau shows that this area largely transitioned into a semi-arid region, with the boundary between the semi-arid and semi-humid areas in northern China shifting significantly southeastward (Zheng *et al.*, 2013).

Moreover, in the northeastern region, from 1980 to 2010, the 400 mm precipitation isohyet in China retreated significantly southeastward. Li *et al.* (2019) also observed a drying trend in 4.58% of the global land area over a longer timescale (1948–2008), which was primarily concentrated in northern China and tropical Africa. Furthermore, the increasing severity of drought in arid areas, as indicated by the trend of the aridity index (AI), is linked to desertification (Zhang *et al.*, 2024). Previous research highlighted that global warming is intensifying the expansion of existing arid regions, a process driven not only by reduced moisture but also by the alteration by the same arid regions of the climate conditions in downwind areas, which further promotes their desertification (Koppa *et al.*, 2024).

There is clearly a broad consensus in literature on the expansion of arid regions; however, a controversy remains on the mechanisms driving the expansion of drought areas. Therefore, future research should adopt a more systematic perspective, investigating the mechanisms driving arid region changes from the local climate, atmospheric circulation and sea surface temperature variations. Moreover, overall, the boundary change detection method proved to be able to effectively quantify the spatial and temporal variation characteristics of China's 400 mm isohyet across different periods. In addition, this method was showed to be applicable to the quantitative study of the directions of spatial and temporal variation and of the distances of linear geographical elements, offering promising applications. However, it is important to note that this study relied on high-density data from Chinese meteorological observation stations. Considering that a generalized application of the isohyet detection method in other regions globally may be constrained by the completeness of regional observational data, it is still necessary to leverage the high spatial and temporal resolution and spatial coverage capabilities of remote sensing imagery, exploring the integration of field observations with remote sensing data. A series of studies have been conducted on global drought area changes (Tariq *et al.*, 2024; Huang *et al.*, 2016b; Yao *et al.*, 2020), and it is projected that in the next 70 years, global arid regions may continue to expand, with the area of drought regions potentially increasing by 4.1%–10.6% (Liu *et al.*, 2023). However, some scholars argued that there is an overestimation in the ecological hydrological index changes simulated by the AI, and under future global warming, the changes in the global arid region area may be minimal (Berg and McColl, 2021). Therefore, future trends in drought changes remain highly uncertain, making it difficult to find a unified consensus.

Through the precise quantification of multidirectional displacements of the 400 mm precipitation isohyet, the results of this study can provide the following types of support for climate adaptation and management. First, they can play a role in guiding the early warning systems for floods and droughts, as well as in the long-term planning of agricultural zoning, water resource management, and ecological protection. Second, the detailed detection model of precipitation isohyet, proposed in this study, can serve as a key knowledge basis to improve regional climate models, thereby enhancing the reliability of future predictions. Third, the findings of this study may serve as the basis for the development of region-specific, data-driven policy frameworks to mitigate social and economic risks (such as the livelihood security of agricultural and pastoral communities), and to promote resilient land use planning in the context of ongoing climate change.

5. Conclusion

This study confirmed that the interpolation method has a high accuracy, as well as good reliability and applicability in the spatialization of precipitation data in China. The temporal and spatial scale effects of the spatial fluctuations of China's 400 mm precipitation isohyet were found to be significant. Regionally, the 400 mm precipitation isohyet in the eastern part of China showed a significant westward shift and a slight southward shift, while in the western region it exhibited an eastward and northward shift, with the latter being significant. As for agricultural regions, LPR exhibited a significant southward shift.

Since 1961, the spatial variation of China's 400 mm isohyet has generally been stable, with occasional intense fluctuations. The most significant fluctuations occurred in the border areas between Heilongjiang, Jilin and Inner Mongolia, followed by the Tibetan Plateau. In terms of temporal variations, the fluctuations of the QTR isohyet exhibited a pattern characterized by low values at both ends, and high values in the middle. Overall, compared to the 1960s, the 2010s showed a slight warming and wetting trend in the isohyet across the QTR, the NECR and the Hexi Corridor, while the LPR and the MGR exhibited the opposite trend. From the 1980s to the 2000s, there was a clear warming and drying trend in the northeastern regions. In contrast, compared to the 2000s, the 2010s showed a warming and wetting trend in the climate of the NECR, the MGR, the LPR, and the QTR.

References

Amrouni, O., Hzami, A. and Heggy, E. (2019), "Photogrammetric assessment of shoreline retreat in North Africa: anthropogenic and natural drivers", *ISPRS Journal of Photogrammetry and Remote Sensing*, Vol. 157, pp. 73-92.

Andrew, C.C. and Bill, B. (2002), "Variability and spatial modeling of fine-scale precipitation data for the Sonoran Desert of south-west Arizona", *Journal of Arid Environments*, Vol. 50, pp. 573-592.

Berg, A. and McColl, K.A. (2021), "No projected global drylands expansion under greenhouse warming", *Nature Climate Change*, Vol. 11 No. 4, pp. 331-337.

Che, Y.J., Guan, X.C., Wang, S.J. and Wu, R. (2020), "Spatial variation analysis of the 800 mm isohyet in the monsoon region of eastern China", *Plateau Meteorology*, Vol. 39 No. 5, pp. 997-1006.

Chen, F.R., Wang, Y.G. and Li, X. (2024), "A data- and knowledge-driven method for fusing satellite-derived and ground-based preicpitation observations", *IEEE Transactions on Geoscience and Remote Sensing*, Vol. 62 No. 4, pp. 1-13.

Ding, Y.H., Liu, Y.J., Xu, Y., Wu, P., Xue, T., Wang, J., Shi, Y., Zhang, Y.X., Song, Y.F. and Wang, P.L. (2023), "Regional responses to global climate change: progress and prospects for trend, causes, and projection of climatic warming-wetting in Northwest China", *Advances in Earth Science*, Vol. 38 No. 6, pp. 551-562.

Du, J.K., Qiu, Y.Q., Li, Y.L., Lu, Q., Hao, C.F. and Liu, H.Y. (2023), "Evolution characteristics of the interannual and intra- annual precipitation in China from 1956 to 2016", *Advances in Water Science*, Vol. 34 No. 2,
pp. 182-196.

Gao, Y.H., Xu, J.W. and Zhang, M. (2020), "Advances in the study of the 400 mm isohyet migrations and wetness and dryness changes on the Chinese mainland", *Advances in Earth Science*, Vol. 35 No. 11, pp. 1101-1112.

Held, I.M. and Soden, B.J. (2006), "Robust responses of the hydrological cycle to global warming", *Journal of Climate*, Vol. 19 No. 21, pp. 5686-5699.

Hsu, H. and Fueglistaler, S. (2025), "Robust projections of changing precipitation evenness in a warming climate", *Geophysical Research Letters*, Vol. 52 No. 9, pp. 1-11.

Huang, J.P., Yu, H.P., Dai, A., Wei, Y. and Kang, L. (2017), "Drylands face potential threat under 2°C global warming target", *Nature Climate Change*, Vol. 7 No. 6, pp. 417-422.

Huang, J.P., Ji, M.X., Xie, Y.K., Wang, S.S., He, Y.L. and Ran, J.J. (2016a), "Global semi-arid climate change over last 60 years", *Climate Dynamics*, Vol. 46 Nos 3-4, pp. 1131-1150.

Huang, J.P., Yu, H.P., Guan, X.D., Wang, G.Y. and Guo, R.X. (2016b), "Accelerated dryland expansion under climate change", *Nature Climate Change*, Vol. 6 No. 2, pp. 1-7.

Hutchinson, M.F. and Xu, T. (2013), "Anusplin version 4.4 user guide", available at: http://fennerschool.anu.edu.au/files/anusplin44.pdf

IPCC (2021), Climate Change 2021: the Physical Science Basis, the Working Group I contribution to the Sixth Assessment Report.

Koppa, A., Keune, J., Schumacher, D.L., Michaelides, K., Singer, M., Seneviratne, S. and Mirales, D.G. (2024), "Dryland self-expansion enabled by land–atmosphere feedbacks", *Science*, Vol. 385 No. 6712, pp. 967-972.

Li, Y., Chen, Y. and Li, Z. (2019), "Dry/wet pattern changes in global dryland areas over the past six decades", *Global and Planetary Change*, Vol. 178, pp. 184-192.

Li, Y.Y., Li, Y.L., Guo, X.N., Pan, Z.R. and Liu, W.F. (2025), "Spatial-temporal distribution and variation characteristics of precipitation in China during 1956-2016", *Advances in Water Science*, Vol. 36 No. 1, pp. 1-17.

Liepert, B. and Romanou, A. (2005), "Global dimming and brightening and the water cycle", *Bulletion of the American Meteorology Society*, Vol. 86, pp. 622-623.

Liu, J.H., Gao, J.X. and Geng, B. (2007), "Study on the dynamic change of land use and landscape pattern in the farming-pastoral region of Northern China", *Research of Environmental Sciences*, Vol. 20 No. 5, pp. 148-154.

Liu, K., Li, X., Wang, S. and Zhou, G. (2023), "Past and future adverse response of terrestrial water storages to increased vegetation growth in drylands", *Npj Climate and Atmospheric Science*, Vol. 6 No. 1, p. 113.

Liu, Z.J., Yu, X.X., Wang, S.S. and Shang, G. (2012), "Comparison of three covariate methods for precipitation interpolation accuracy in thin-plate smoothing spline interpolation", *Progress in Geography*, Vol. 31 No. 1, pp. 56-62.

Lu, F.Z. and Lu, H.Y. (2019), "Ahigh-resolution grid dataset of air temperature and precipitation for Qinling-Daba Mountains in central China and its implications for regional climate", *Acta Geographica Sinica*, Vol. 74 No. 5, pp. 875-888.

Prăvălie, R., Bandoc, G., Patriche, C. and Sternberg, T. (2019), "Recent changes in global drylands: evidences from two major aridity databases", *CATENA*, Vol. 178, pp. 209-231.

Tariq, A., Sardans, J., Zeng, F., Graciano, C., Hughes, A.C., Farré-Armengol, G. and Peñuelas, J. (2024), "Impact of aridity rise and arid lands expansion on carbon-storing capacity, biodiversity loss, and ecosystem services", *Global Change Biology*, Vol. 30 No. 4, p. e17292.

Treppiedi, D., Villarini, G., Bender, J. and Valerio, L. (2025), "Precipitation extremes projected to increase and to occur in different times of the year", *Environmental Research Letters*, Vol. 20 No. 1, p. 014014.

Wahba, G. and Wendelberger, J. (1980), "Some new mathematical methods for variational objective analysis using splines and cross validation", *Monthly Weather Review*, Vol. 108 No. 8, pp. 1122-1143.

Wang, J.S., Chen, F.H., Jin, L.Y. and Guo, J.Y. (2008), "Relationship between climate anomalies in the arid regions of Central and East Asia and sea-level pressure anomalies over the past 100 years", *Plateau Meteorology*, Vol. 27 No. 1, pp. 84-95.

Wang, H., Yan, D.H., Qin, D.Y. and Wang, J.H. (2005), "Spatial variation of the 400 mm isohyets in the yellow river basin over the past 50 years", *Advances in Earth Science*, Vol. 20 No. 6, pp. 649-655.

Yao, J., Liu, H., Huang, J., Gao, Z.M., Wang, G.Y., Li, D., Yu, H.P. and Chen, X.Y. (2020), "Accelerated dryland expansion regulates future variability in dryland gross primary production", *Nature Communication*, Vol. 11, p. 1665.

Yuan, Z., Yan, D.H., Yang, Z.Y., Jun, Y. and Yong, Y. (2014), "Temporal and spatial changes of 400 mm and 800 mm isohyets in China from 1961 to 2010", *Advances in Water Science*, Vol. 25 No. 4, pp. 494-502.

Zhang, X., Evans, J.P. and Burrell, A.L. (2024), "Less than 4% of dryland areas are projected to desertify despite increased aridity under climate change", *Communications Earth and Environment*, Vol. 5 No. 1.

Zhao, J., Chen, Y.W., Han, Y.F., Li, Z., Liu, Y.Z. and Li, W. (1993),. *Physical Geography of China*, (3rd Edition)., Higher Education Press, Beijing.

Zhao, H., Huang, W., Xie, T., Wu, X., Xie, Y.W., Feng, S. and Chen, F.H. (2019), "Optimization and evaluation of a monthly air temperature and precipitation gridded dataset with a 0.025° spatial resolution in China during 1951-2011", *Theoretical and Applied Climatology*, Vol. 138 Nos 1-2, pp. 491-507.

Zheng, J.Y., Bian, J.J., Ge, Q.S., Hao, Z.X. and Yin, Y.H. (2013), "The climate regionalization in China for 1981-2010", *Chinese Science Bulletin*, Vol. 58 No. 30, pp. 3088-3099.

Zheng, D., Wu, S.H., Yin, Y.H., Yang, Q.Y., Zhao, D.S. and Zhang, X.Q. (2016), "Frontiers in the study of natural regional systems in China under global change", *Acta Geographica Sinica*, Vol. 71 No. 9, pp. 1475-1483.

Supplementary material

The supplementary material for this article can be found online.

Corresponding author

Yaochen Qin can be contacted at: qinyc@henu.edu.cn